Automated Identification and Quantification of Subretinal Fibrosis in Neovascular Age-Related Macular Degeneration Using Polarization-Sensitive OCT

Philipp Roberts,[1] Mitsuro Sugita,[2,3] Gábor Deák,[1] Bernhard Baumann,[2] Stefan Zotter,[2] Michael Pircher,[2] Stefan Sacu,[1] Christoph K. Hitzenberger,[2] and Ursula Schmidt-Erfurth[1]

[1]Department of Ophthalmology and Optometry of the Medical University of Vienna, Vienna, Austria
[2]Center for Medical Physics and Biomedical Engineering of the Medical University of Vienna, Vienna, Austria
[3]Canon, Inc., Tokyo, Japan

Correspondence: Ursula Schmidt-Erfurth, Department of Ophthalmology and Optometry of the Medical Univeristy of Vienna, Waehringer Guertel 18-20, 1090 Vienna, Austria; ursula.schmidt-erfurth@meduniwien.ac.at.

Submitted: November 21, 2015
Accepted: February 9, 2016

Citation: Roberts P, Sugita M, Deák G, et al. Automated identification and quantification of subretinal fibrosis in neovascular age-related macular degeneration using polarization-sensitive OCT. *Invest Ophthalmol Vis Sci*. 2016;57:1699–1705. DOI:10.1167/iovs.15-18694

Purpose. To identify and quantify subretinal fibrosis in eyes with advanced neovascular age-related macular degeneration (nAMD) using polarization-sensitive optical coherence tomography (PS-OCT).

Methods. Eyes of patients with subretinal fibrosis secondary to nAMD were included in this case series. All patients underwent a complete ophthalmic examination to clearly identify advanced nAMD lesions with fibrosis. Examinations of PS-OCT were performed using a novel system with an integrated eye tracker. Areas of fibrosis in PS-OCT, automatically segmented using a custom-built algorithm, were compared with conventional imaging modalities including spectral-domain OCT, fluorescein angiography, and color fundus photography in their potential to visualize fibrosis in nAMD.

Results. Fifteen eyes of 15 consecutive patients were included. In polarization-sensitive OCT B-scans, a distinct "column-like" pattern was observed in averaged axis orientation images. En face analysis provided a precise mapping of the fibrotic scar component. Fibrous tissue was selectively identified by PS-OCT based on birefringence in all lesions, whereas in SD-OCT, subretinal hyperreflective material (SHRM) could not be further classified into scar tissue, fibrovascular material, or other AMD-specific material. Based on simultaneous polarization analyses in PS-OCT, the level of RPE alteration could be evaluated as well, showing thinning and loss of RPE associated with subretinal fibrosis.

Conclusions. Using PS-OCT, subretinal fibrosis can be identified as an intrinsically birefringent structure and can be segmented based solely on tissue-specific contrast. Polarization-sensitive OCT offers a unique method to identify clinically relevant components of SHRM (i.e., neovascular tissue versus fibrous tissue) and therefore allows for an optimized disease management and evaluation of therapeutic strategies.

Keywords: polarization-sensitive optical coherence tomography, fibrosis, subretinal hyperreflective tissue, choroidal neovascularization, age-related macular degeneration

Neovascular age-related macular degeneration (nAMD) is still one of the most common vision-threatening diseases of the elderly population.[1–5] Despite effective treatment strategies, which have been established within recent years, complications of advanced AMD such as hemorrhage, geographic atrophy, or fibrosis lead to irreversible visual impairment.[6,7] Particularly, subretinal fibrosis is a common feature of advanced neovascular disease and strongly determines the prognosis even with adequate therapy. Differentiating between active neovascular tissue and irresponsive fibrous tissue—characterizing an end stage of disease beyond treatment—is extremely difficult using standard imaging modalities. Multimodal imaging including color fundus photography (CF) and invasive technologies such as fluorescein angiography (FA) or indocyanine green angiography (ICGA), is to date the only way to approach end-stage lesions in AMD.[6,8,9] Ever since the introduction of spectral-domain optical coherence tomography (SD-OCT) in ophthalmology,[10] the means of diagnosis and monitoring of patients with nAMD have changed drastically, from a clinical (fundoscopy) or angiographic (leakage in FA) approach to a more distinct, noninvasive morphologic (SD-OCT) approach. Spectral-domain OCT enables visualization of the retinal layers and adjacent tissues in close-to-microscopic resolution; however, discriminating different tissues with similar reflectivity (e.g., different components of subretinal hyperreflective material) is challenging.[11] In eyes with nAMD, subretinal fibrosis as a late-stage complication is observed more commonly in type II (subretinal) choroidal neovascularization (CNV) than in type I (sub-retinal pigment epithelial [RPE]) CNV and is often characterized in SD-OCT as subretinal hyperreflective material (SHRM).[6] However, only in combination with CF can fibrosis be diagnosed, as the components of SHRM (e.g., lipofuscin, subretinal hemorrhage, neovascular tissue, fibrosis) cannot be differentiated by conventional SD-OCT.[12–14]

Investigative Ophthalmology & Visual Science

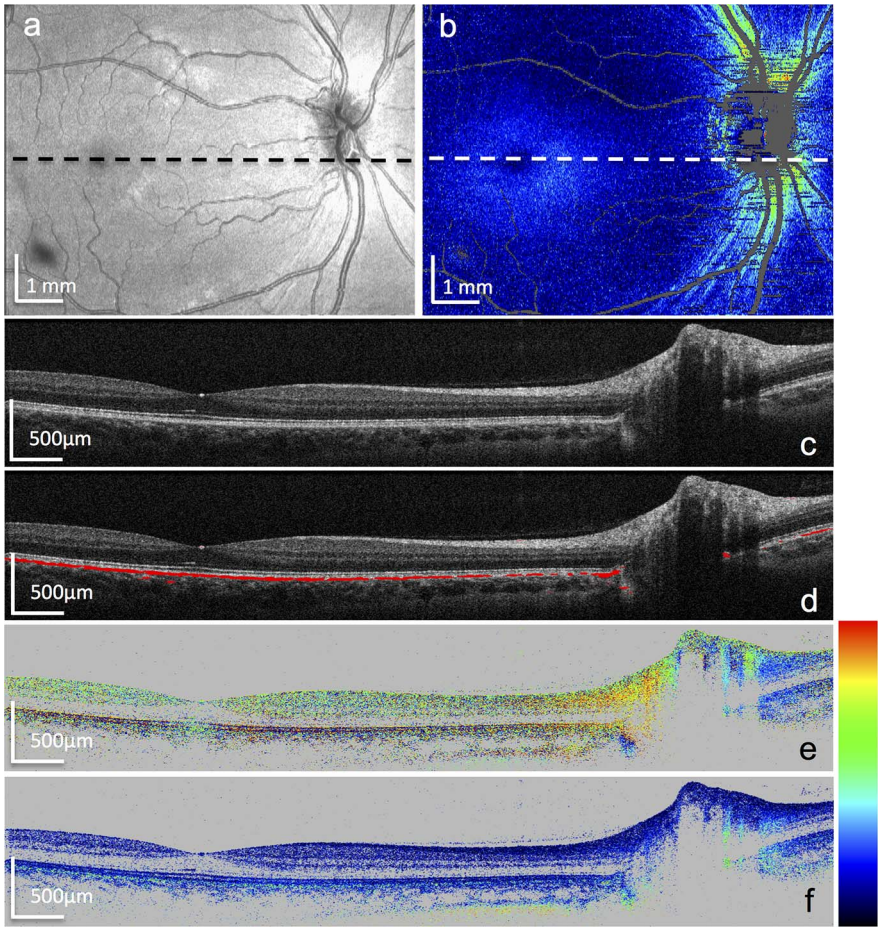

Figure 1. Polarization-sensitive OCT imaging of the right eye of a healthy person. En face images show pseudo-SLO (**a**) and retardation (**b**) imaging. Location of the intensity (**c**), depolarizing material overlay (**d**), axis orientation (**e**), and retardation (**f**) single frame B-scans are indicated by the *dashed lines*. *Color scales*: 0 to 50° for retardation (**b**, **f**); −90 to +90° for axis orientation (**e**).

Polarization-sensitive (PS)-OCT, an extension of SD-OCT, offers segmentation of different layers of the ocular fundus based solely on tissue-specific contrast.[15] In the human eye, three distinct physical properties can be distinguished using PS-OCT, namely: depolarization (e.g., RPE, birefringence [e.g., retinal nerve fiber layer], and polarization preservation [e.g., photoreceptor layers]). It has been shown that different types of tissue that appear indistinguishable by conventional OCT can be differentiated and segmented using PS-OCT based on tissue-specific properties.[16–19] In dermatologic studies, scar tissue has been shown to cause a distinct increase in birefringence in PS-OCT imaging originating from the inherent arrangement of collagenous fibers.[20,21] In the ocular setting, birefringence is a typical feature of subretinal fibrosis, as shown in previous studies.[22–24] In management of AMD, reliable identification of fibrosis by PS-OCT could help differentiate between patients with subretinal neovascular tissue who are in need of continued therapy and patients with inactive scar lesions who would not benefit from further therapeutic intervention. Furthermore, with combination treatments underway presumably preventing fibrosis, PS-OCT might represent an objective and convenient modality to reliably detect and quantify fibrous tissue and the realistic impact of treatment.[25,26]

The purpose of this study was to identify and automatically segment subretinal/sub-RPE fibrotic scarring in eyes with advanced nAMD by PS-OCT, exploiting the tissue-specific, birefringent properties of fibrous material in a noninvasive and quantitative way.

Patients and Methods

The study protocol was approved by the local ethics committee and adhered to the ethical tenets of the Declaration of Helsinki. Patients gave written informed consent prior to study inclusion, clinical examination, and patient selection. Fifteen eyes of 15 consecutive patients with subretinal or sub-RPE fibrosis in advanced nAMD were included in this case series. The diagnosis of fibrosis was based on clinical examination, CF, and FA. Patients with active CNV, ocular media opacification, or retinal disease other than late-stage AMD were not included in this study. Patients who had received intravitreal anti-VEGF medication within 12 months prior to screening were not included in the study. Examinations included best corrected visual acuity (BCVA); dilated fundus examination; SD-OCT (Cirrus high-definition [HD]-OCT; Carl Zeiss Meditec, Dublin, CA, USA); FA (Spectralis HRA+OCT imaging device; Heidelberg Engineering, Heidelberg, Germany); CF (Optos Optomap P200Tx and FF 450plus; Carl Zeiss Meditec); and PS-OCT. Conventional retinal imaging methods were compared to PS-OCT.

Fibrosis was defined as whitish or yellowish subretinal tissue in fundoscopy that was not related to drusen, hard

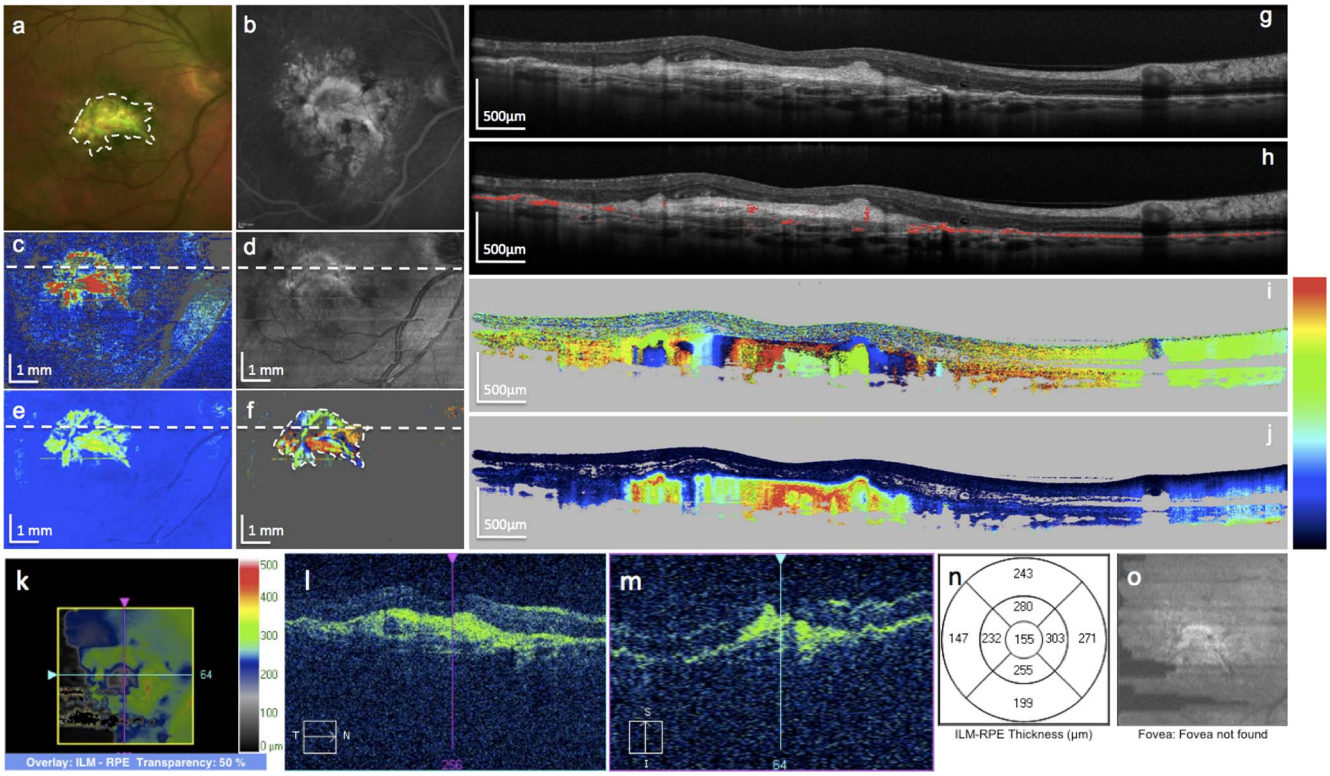

Figure 2. Color fundus photography (**a**), late phase fluorescein angiography (**b**), PS-OCT imaging (**c**–**j**), and conventional SD-OCT imaging (**k**–**o**) of the right eye of a patient with subretinal fibrosis secondary to neovascular AMD. Retardation en face (**c**), pseudo–scanning laser ophthalmoscope (SLO) (**d**), median retardation en face (**e**), and the axis en face map thresholded by median retardation (**f**) show similarity with standard imaging (**a**, **b**). In the averaged intensity (**g**), depolarizing material (**h**), axis orientation (**i**), and retardation B-scans (**j**) from PS-OCT the scar complex can be observed as subretinal hyperreflective and birefringent tissue. The retinal pigment epithelium is absent in the area of fibrosis (**h**); however, clusters of depolarizing material are consistent with pigment accumulations in (**a**). Note the "column-like" pattern in the axis orientation B-scan image (**i**) reflecting the intrinsic birefringence pattern of collagenous fibers in fibrous tissue. Tracings from PS-OCT segmentation (**f**) were overlayed on color fundus photography (**a**) to facilitate the comparison between the two imaging modalities. The retinal thickness map (**k**), central horizontal (**l**), and vertical (**m**) B-scans as well as an ETDRS-grid with retinal thickness (**n**), and the pseudo-SLO (**o**) of the fibrous lesion generated from conventional SD-OCT (Carl Zeiss Meditec) are shown for comparison. *Color scales*: 0 to 50° for retardation en face (**c**), −90 to +90° for axis orientation (**f**, **i**), 0 to +90° for median retardation (**e**), and retardation B-scan (**j**).

exudates, fibrin, or dehemoglobinized blood and was associated with early hypofluorescence and late staining in FA.

PS-OCT Imaging

A homemade spectral-domain PS-OCT prototype developed at the Center for Medical Physics and Biomedical Engineering at the Medical University of Vienna in cooperation with Canon, Inc., (Tokyo, Japan) incorporating a line-scanning laser ophthalmoscopy channel for retinal tracking was used in this study. A detailed description of the system can be found in Sugita et al.[27] In brief, a superluminescent diode (center wavelength: 863 nm; full width half maximum bandwidth: 60 nm) was used as a light source and fed into a Michelson interferometer using polarization-maintaining fiber optics. The eye was illuminated by circularly polarized light. The polarization-sensitive detection unit featured two identical spectrometers (i.e., one for each orthogonal polarization channel) that were read simultaneously at 70 kHz line rate. Raster scanning was performed over 28° (x) × 21° (y), corresponding to a field of view of approximately 8 × 6 mm on the retina. Polarization-sensitive OCT data sets comprising 250 B-scans with 1024 A-scans were recorded at a volume acquisition speed of 4.5 seconds. At selected locations, 83 repeated B-scans were acquired to compute averaged PS-OCT images with higher signal-to-noise ratio and improved polarization contrast.

In addition to PS-OCT, the system featured a line-scanning laser ophthalmoscope (LSLO) channel. A line-shaped laser beam at 786-nm wavelength was scanned perpendicularly over the retina (i.e., in y-direction) at variable rates of 1 to 60 Hz. Light backscattered from the retina was detected by a charge-coupled device line scan camera at 70 kHz. Images of LSLO and PS-OCT were acquired simultaneously. By matching LSLO images to a template, transverse eye motion was tracked in real time and compensated by applying steering offsets to the galvanometer scanners accordingly.

Images of PS-OCT (reflectivity, phase retardation, optic axis orientation) were computed from the raw data.[28] In order to compensate for polarization artifacts induced by the birefringent cornea, a Jones matrix based algorithm was used.[29] In addition to PS-OCT images displaying birefringent tissue properties (i.e., phase retardation and optic axis orientation), degree of polarization uniformity (DOPU) images were also computed.[30] Images of DOPU enable identification and segmentation of tissues such as the RPE based on the light depolarizing property of melanin pigments.[17,30–36]

A representative example of a healthy eye imaged by the PS-OCT device is illustrated in Figure 1.

PS-OCT Imaging of Fibrosis

A custom-built algorithm was used for automated identification of fibrosis, which works in the following way:

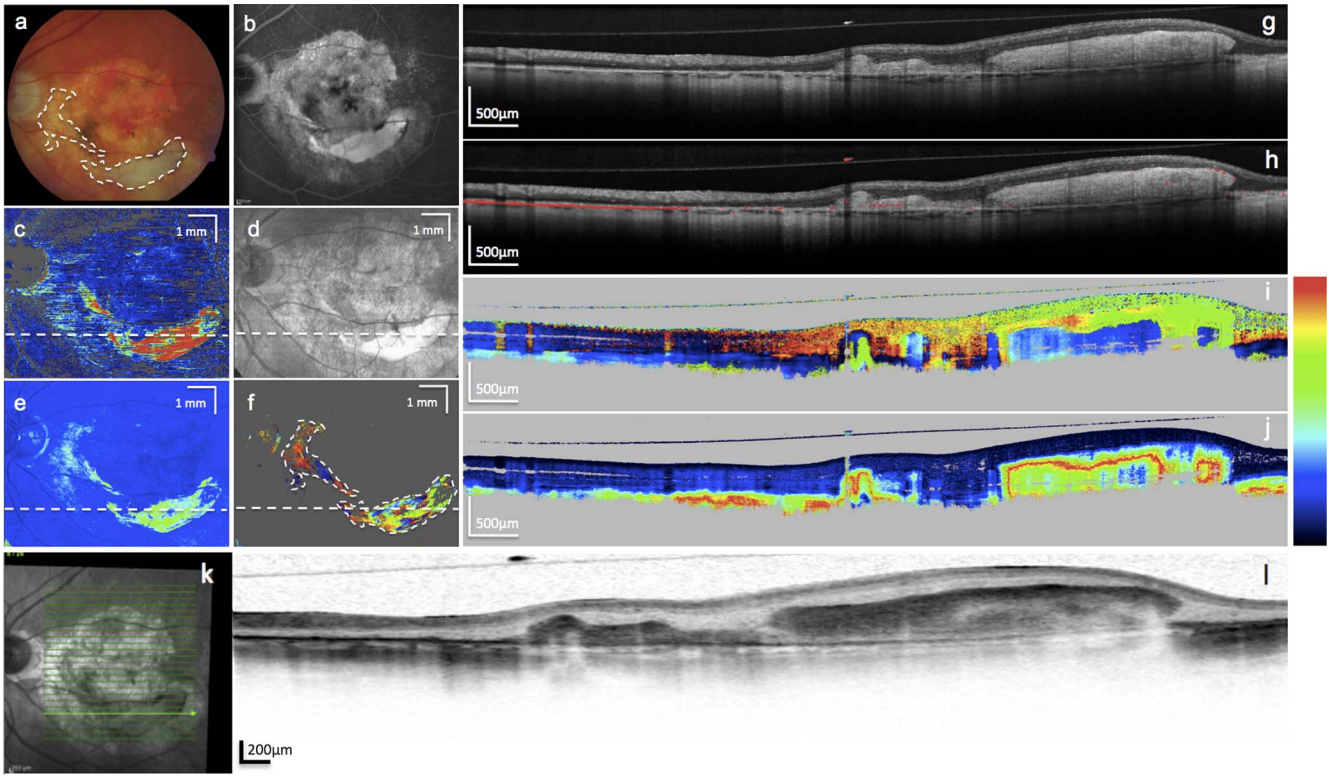

Figure 3. Color fundus photography (**a**), late-phase fluorescein angiography (**b**), PS-OCT imaging (**c**–**j**), and conventional SD-OCT imaging (**k**, **l**) of the left eye of a patient with subretinal fibrosis secondary to neovascular AMD. Retardation en face (**c**), pseudo-SLO (**d**), median retardation en face (**e**), and the axis en face map thresholded by median retardation (**f**) show similarity with standard imaging (**a**, **b**). In the averaged intensity (**g**), depolarizing material (**h**), axis orientation (**i**), and retardation B-scans (**j**) from PS-OCT the scar complex can be observed as subretinal hyperreflective and birefringent tissue. Tracings from PS-OCT segmentation (**f**) were overlayed on color fundus photography (**a**) to facilitate the comparison between the two imaging modalities. The infrared SLO en face image (**k**) as well as a conventional SD-OCT B-scan (Heidelberg Engineering) are shown for comparison. *Color scales*: 0 to 50° for retardation en face (**c**), −90 to +90° for axis orientation (**f**, **i**), 0 to +90° for median retardation (**e**), and retardation B-scan (**j**).

En face PS-OCT images were computed from the image stacks. Only pixels exceeding a user-set threshold in the reflectivity images were considered. Average retardation as well as median retardation was calculated along each A-scan and then mapped to a two-dimensional (2D) fundus image. Average axis orientation was computed by axial phasor averaging along each A-line as described in Gotzinger et al.[37] and mapped to a 2D image. To provide a clear distinction of the axis orientation characteristics of fibrotic (i.e., collagenous) tissue in the fundus, areas with low median retardation values (less than 30°) were masked in gray. All en-face images—OCT fundus projection images, phase retardation en face maps, and axis orientation en-face maps—represent projections along the entire depth range. Since the penetration depth was limited, mostly signals from retinal tissue contributed to these maps.

Results

Fifteen eyes of 15 consecutive patients (nine female, six male) with a mean age of 79 ± 7 years (± standard deviation) were included in this observational case series. Subretinal/-RPE fibrosis with staining typical of scar tissue in late FA was mandatory in all patients. In all eyes presenting subretinal fibrosis, thinning/loss of the RPE layer was observed by PS-OCT in the areas of subretinal scarring. Disseminated depolarizing particles were present within the subretinal scar complex, presumably remnants of dissociated RPE cells. In general, an intact RPE-layer (a continuous single cell layer below the neuroretina) was not detected in any region where subretinal fibrosis had occurred (Fig. 2).

In the averaged axis orientation B-scan images, a distinct pattern of well-defined regions (columns) of uniform axis orientation (similarly colored blocks) was observed in areas of fibrosis, indicating the orientation of the collagenous fibers within the scar tissue (Fig. 2). These patterns were observed in all eyes with fibrosis in averaged PS-OCT axis orientation B-scans (Supplementary Figs. S5–19). The "columns" seen in these B-scans were actually caused by projections of the axis within the fibrous tissue on structures located posterior, comparable with the shadowing effect caused by blood vessels in SD-OCT B-scans.

Subretinal/-RPE hyperreflective material other than fibrous tissue (e.g., drusen material, neovascular tissue, blood) did not exhibit this column-like pattern in the axis orientation B-scans (Supplementary Figs. S20, S21).

Using en face PS-OCT images, it was possible to compare areas of subretinal fibrosis to conventional imaging modalities in 9 eyes (60%). In these eyes, the area of fibrosis as segmented automatically by PS-OCT corresponded well to the area of ophthalmoscopically visible whitish scar tissue in CF and the area of late staining in fundus angiography (Figs. 2, 3).

In three out of these nine eyes, a massive scar complex was exceeding the field of view of the PS-OCT device (Fig. 4); however, the imaged portion of the fibrosis was always detected correctly, showing reliability of the method even in end-stage cases with extensive tissue destruction.

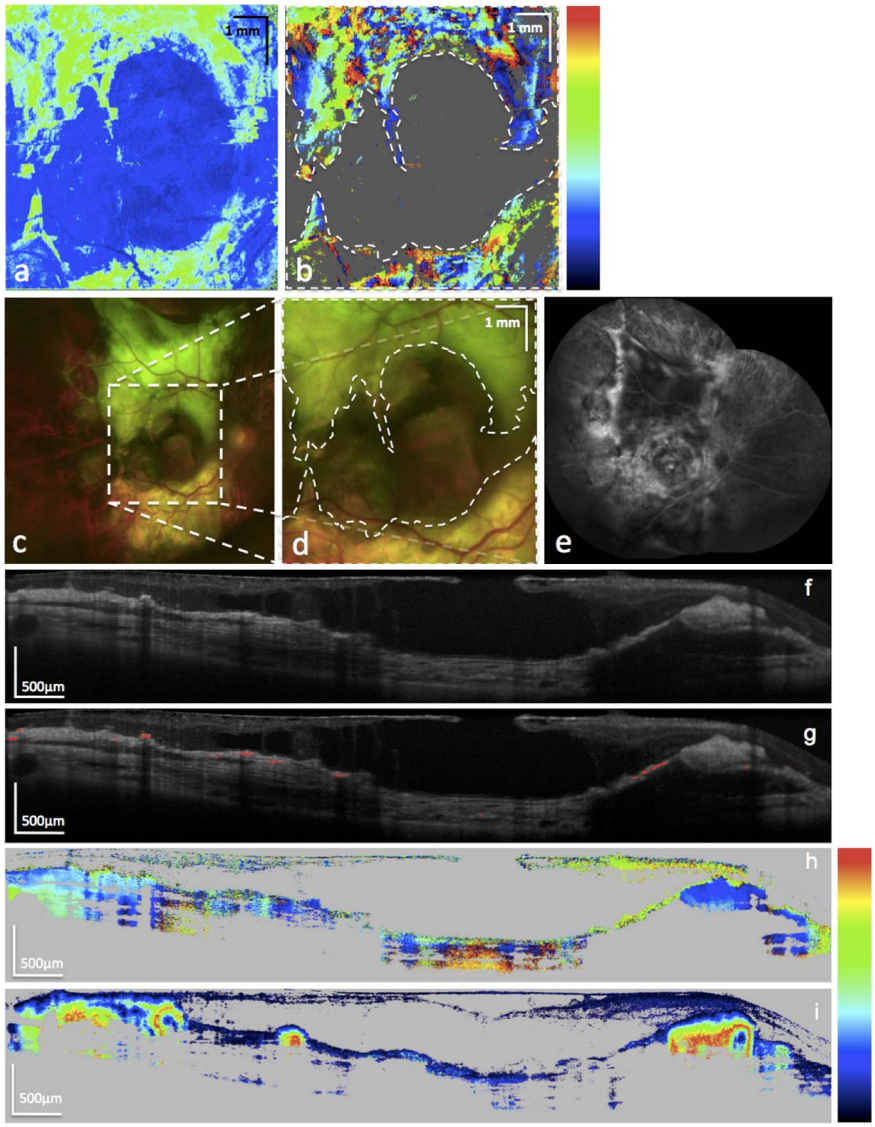

FIGURE 4. Median retardation en face map (**a**), axis en face map thresholded by median retardation (**b**) imaged by PS-OCT, color fundus photography (**c**) magnified in (**d**) and fluorescein angiography (**e**) of the right eye of a patient with extensive subretinal fibrosis secondary to neovascular AMD. The averaged foveal PS-OCT B-scans (**f–i**) show a severe alteration of the retinal contour and structure. Subretinal hyperreflective material can be observed in the intensity B-scan (**f**) and depolarizing material segmentation overlay B-scan (**g**). Tracings from PS-OCT segmentation (**b**) were overlayed on color fundus photography (**d**) to facilitate the comparison between the two imaging modalities. A loss of RPE can be noted, as well. Birefringent material can be identified in the axis orientation (**h**) and retardation B-scan (**i**). *Color scales*: 0 to +90° for median retardation (**a**), −90 to +90° for axis orientation (**b**, **h**), 0 to 90° for retardation (**i**).

In 6 eyes (40%), a clear delineation of the fibrous tissue in en face view was not possible. This was due to the axial extension of the fibrosis exceeding the depth of the PS-OCT B-scan (one eye), blinking artifacts (one eye), a failure of the cornea compensation (2 eyes) or a segmentation error in the automatic algorithm caused by attenuated signal to noise ratio (2 eyes). However, in the averaged PS-OCT B-scans, the fibrous tissue was clearly detectable in all eyes based on intrinsic birefringence.

DISCUSSION

This study was aiming to evaluate PS-OCT as a new imaging modality to noninvasively identify scarring at the ocular fundus in advanced AMD based on tissue birefringence. This optical phenomenon, which allows the detection of fibrosis, was shown in dermatologic studies using PS-OCT. Furthermore, it had been shown that the higher the content of ordered collagen fibers in a tissue, the more rapid the change of the polarization state of the probing light beam along the depth direction and the higher the phase retardation rates.[21] This property of fibrous tissue could also be exploited in ophthalmology in order to identify scarring of (sub)-retinal lesions in nAMD.[22–24] In this prospective study, performed in well-phenotyped eyes with advanced disease, a specific pattern of a column-like collagen appearance was visualized in all cases (n = 15 eyes) in eye-tracked and averaged PS-OCT axis orientation B-scans. The pattern originated from the structural arrangement of collagen fibers within the fibrous scar. Depending on the direction of these fibers within the imaged area, the birefringent signal originating from the scar tissue changed. This phenomenon has been observed in PS-OCT imaging studies of scarring in skin tissue and might offer a new

Investigative Ophthalmology & Visual Science

way to differentiate inert fibrous and active neovascular tissue noninvasively.[20,21] In the study described herein, eye-tracked en face retardation maps clearly showed fibrous tissue and could be directly compared with scar features in CF and angiographic images in the majority of the study eyes ($n = 9$; 60%).

Substantial interest has been directed toward SHRM during recent years and studies are attempting to characterize this feature in SD-OCT and interpret the change of SHRM as a response to antineovascular treatment. In general, a decrease of the volume of SHRM is considered beneficial for retinal function and authors attributed such a reduction to the effect of treatment.[11,14] However, as the various components of such hyperreflective masses imaged in conventional SD-OCT preclude identification of neovascular complex, exudative material from CNV leakage, fibrous tissue, or blood, of which some are sequelae of active disease while others may represent irresponsive scarring, a mere reduction of SHRM does not offer understanding of lesion biology. The presence of fibrous tissue in eyes with treatment-naïve nAMD significantly adversely influences the response to treatment. Therefore, the detection of scarring before the initiation of treatment is of great clinical importance and has a direct impact on the individual prognosis. With ongoing research, birefringence generated by scar tissue might be specifically targeted in the future in order to differentiate active CNV lesions from stable fibrous complexes as one element in noninvasive multimodal imaging including OCT angiography. Formation of fibrosis could be detected at an earlier stage and, with new treatment strategies in the pipeline, might be tackled or stopped, resulting in better functional outcome for the patient.[26] Polarization-sensitive OCT is currently the only promising modality to evaluate fibrosis in advanced AMD in a reliable qualitative and quantitative manner as opposed to conventional intensity-based SD-OCT depicting a conglomerate of various active and inactive components. In addition to imaging the fibrous component, PS-OCT simultaneously offers selective three-dimensional imaging of the condition of the RPE layer, which is very challenging in conventional OCT imaging. Geographic atrophy (GA) is the other major feature associated with vision loss in advanced AMD.[38] Focal association or dissociation of fibrosis and RPE atrophy may clarify the pathophysiology of GA progression.

Limitations of this study were a limited number of study participants and the limited imaging depth of the PS-OCT device. Fibrosis, in its dimensions can extend far in the z-axis. Using swept-source OCT technology with a light source operating at a 1-μm wavelength could overcome this issue. This technology offers less signal roll-off and improved signal strength with deeper penetration in tissue.

Furthermore, the device used in this study was not capable of taking averaged images of an eye-tracked volume scan of the retina. Comparison of averaged PS-OCT B-scans and single frame images clearly showed the advantage of image averaging in detection of birefringence. Combining the two features of eye tracking and image averaging when recording a volume scan of the retina could greatly improve the detection and quantification of fibrous tissue. As scar tissue is a very plastic and rather irregularly shaped tissue as opposed to the regular arrangement of the layers of the retina, quantification in a two-dimensional way seems insufficient. A quantification and follow-up of the volume of scar tissue could unambiguously show the ability of different treatments to prevent or halt the formation of fibrous material. Further research and improvement of software algorithms provided, using the birefringence information from PS-OCT could offer automated quantification of fibrosis volume.

In conclusion, this study showed that PS-OCT is capable of automatically detecting and quantifying fibrous tissue based on its specific birefringent properties. Polarization-sensitive OCT provides a noninvasive way to differentiate different components of SHRM, thereby defining the stage of disease progression and the prognosis during therapy. This allows for further understanding of the pathomechanisms of AMD, identifies novel targets for optimized therapy and may guide individualized treatment in the age of "precision medicine."

Acknowledgments

Disclosure: **P. Roberts**, Canon, Inc. (F); **M. Sugita**, Canon, Inc. (F); **G. Dèak**, None; **B. Baumann**, Canon, Inc. (F); **S. Zotter**, Canon, Inc. (F); **M. Pircher**, Canon, Inc. (F); **S. Sacu**, None; **C.K. Hitzenberger**, Canon, Inc. (F); **U. Schmidt-Erfurth**, Alcon Laboratories, Inc. (C), Bayer Healthcare (C), Novartis (C), Allergan (C), Boehringer (C)

References

1. Schmidt-Erfurth U, Chong V, Loewenstein A, et al. Guidelines for the management of neovascular age-related macular degeneration by the European Society of Retina Specialists (EURETINA). *Br J Ophthalmol*. 2014;98:1144–1167.
2. Friedman DS, O'Colmain BJ, Munoz B, et al. Prevalence of age-related macular degeneration in the United States. *Arch Ophthalmol*. 2004;122:564–572.
3. Gemmy Cheung CM, Li X, Cheng CY, et al. Prevalence and risk factors for age-related macular degeneration in Indians: a comparative study in Singapore and India. *Am J Ophthalmol*. 2013;155:764–773.
4. Kawasaki R, Yasuda M, Song SJ, et al. The prevalence of age-related macular degeneration in Asians: a systematic review and meta-analysis. *Ophthalmology*. 2010;117:921–927.
5. Smith W, Assink J, Klein R, et al. Risk factors for age-related macular degeneration: pooled findings from three continents. *Ophthalmology*. 2001;108:697–704.
6. Daniel E, Toth CA, Grunwald JE, et al. Risk of scar in the comparison of age-related macular degeneration treatments trials. *Ophthalmology*. 2014;121:656–666.
7. Bloch SB, Lund-Andersen H, Sander B, Larsen M. Subfoveal fibrosis in eyes with neovascular age-related macular degeneration treated with intravitreal ranibizumab. *Am J Ophthalmol*. 2013;156:116–124. e1.
8. Toth LA, Stevenson M, Chakravarthy U. Anti-vascular endothelial growth factor therapy for neovascular age-related macular degeneration: outcomes in eyes with poor initial vision. *Retina*. 2015;35:1957–1963.
9. Schmidt-Erfurth U, Waldstein SM. A paradigm shift in imaging biomarkers in neovascular age-related macular degeneration. *Prog Retin Eye Res*. 2015;50:1–24.
10. Wojtkowski M, Leitgeb R, Kowalczyk A, Bajraszewski T, Fercher AF. In vivo human retinal imaging by Fourier domain optical coherence tomography. *J Biomed Opt*. 2002;7:457–463.
11. Willoughby AS, Ying GS, Toth CA, et al. Subretinal hyperreflective material in the comparison of age-related macular degeneration treatments trials. *Ophthalmology*. 2015;122:1846–1853.e5.
12. Ying GS, Kim BJ, Maguire MG, et al. Sustained visual acuity loss in the comparison of age-related macular degeneration treatments trials. *JAMA Ophthalmol*. 2014;132:915–921.
13. Keane PA, Patel PJ, Liakopoulos S, Heussen FM, Sadda SR, Tufail A. Evaluation of age-related macular degeneration with optical coherence tomography. *Surv Ophthalmol*. 2012;57:389–414.

14. Shah VP, Shah SA, Mrejen S, Freund KB. Subretinal hyperreflective exudation associated with neovascular age-related macular degeneration. *Retina*. 2014;34:1281–1288.
15. Pircher M, Hitzenberger CK, Schmidt-Erfurth U. Polarization sensitive optical coherence tomography in the human eye. *Prog Retin Eye Res*. 2011;30:431–451.
16. Cense B, Wang Q, Lee S, et al. Henle fiber layer phase retardation measured with polarization-sensitive optical coherence tomography. *Biomed Opt Express*. 2013;4:2296–2306.
17. Baumann B, Baumann SO, Konegger T, et al. Polarization sensitive optical coherence tomography of melanin provides intrinsic contrast based on depolarization. *Biomed Opt Express*. 2012;3:1670–1683.
18. Baumann B, Gotzinger E, Pircher M, et al. Segmentation and quantification of retinal lesions in age-related macular degeneration using polarization-sensitive optical coherence tomography. *J Biomed Opt*. 2010;15:061704.
19. Zotter S, Pircher M, Gotzinger E, et al. Measuring retinal nerve fiber layer birefringence, retardation, and thickness using wide-field, high-speed polarization sensitive spectral domain OCT. *Invest Ophthalmol Vis Sci*. 2013;54:72–84.
20. Pierce MC, Strasswimmer J, Park BH, Cense B, de Boer JF. Advances in optical coherence tomography imaging for dermatology. *J Invest Dermatol*. 2004;123:458–463.
21. Babalola O, Mamalis A, Lev-Tov H, Jagdeo J. Optical coherence tomography (OCT) of collagen in normal skin and skin fibrosis. *Arch Dermatol Res*. 2014;306:1–9.
22. Miura M, Yamanari M, Iwasaki T, et al. Imaging polarimetry in age-related macular degeneration. *Invest Ophthalmol Vis Sci*. 2008;49:2661–2667.
23. Michels S, Pircher M, Geitzenauer W, et al. Value of polarisation-sensitive optical coherence tomography in diseases affecting the retinal pigment epithelium. *Br J Ophthalmol*. 2008;92:204–209.
24. Hong YJ, Miura M, Ju MJ, Makita S, Iwasaki T, Yasuno Y. Simultaneous investigation of vascular and retinal pigment epithelial pathologies of exudative macular diseases by multifunctional optical coherence tomography. *Invest Ophthalmol Vis Sci*. 2014;55:5016–5031.
25. Liegl R, Koenig S, Siedlecki J, Haritoglou C, Kampik A, Kernt M. Temsirolimus inhibits proliferation and migration in retinal pigment epithelial and endothelial cells via mTOR inhibition and decreases VEGF and PDGF expression. *PLoS One*. 2014;9:e88203.
26. Jaffe GJ, Eliott D, Wells JA, Prenner JL, Papp A, Patel SA. A phase 1 study of intravitreous E10030 in combination with ranibizumab in neovascular age-related macular degeneration. *Ophthalmology*. 2016;123:78–85.
27. Sugita M, Zotter S, Pircher M, et al. Motion artifact and speckle noise reduction in polarization sensitive optical coherence tomography by retinal tracking. *Biomed Opt Express*. 2013;5:106–122.
28. Gotzinger E, Pircher M, Hitzenberger CK. High speed spectral domain polarization sensitive optical coherence tomography of the human retina. *Opt Express*. 2005;13:10217–10229.
29. Pircher M, Gotzinger E, Baumann B, Hitzenberger CK. Corneal birefringence compensation for polarization sensitive optical coherence tomography of the human retina. *J Biomed Opt*. 2007;12:041210.
30. Gotzinger E, Pircher M, Geitzenauer W, et al. Retinal pigment epithelium segmentation by polarization sensitive optical coherence tomography. *Opt Express*. 2008;16:16410–16422.
31. Ahlers C, Gotzinger E, Pircher M, et al. Imaging of the retinal pigment epithelium in age-related macular degeneration using polarization-sensitive optical coherence tomography. *Invest Ophthalmol Vis Sci*. 2010;51:2149–2157.
32. Lammer J, Bolz M, Baumann B, et al. Imaging retinal pigment epithelial proliferation secondary to PASCAL photocoagulation in vivo by polarization-sensitive optical coherence tomography. *Am J Ophthalmol*. 2013;155:1058–1067.e1
33. Sayegh RG, Zotter S, Roberts PK, et al. Polarization-sensitive optical coherence tomography and conventional retinal imaging strategies in assessing foveal integrity in geographic atrophy. *Invest Ophthalmol Vis Sci*. 2015;56:5246–5255.
34. Schlanitz FG, Sacu S, Baumann B, et al. Identification of drusen characteristics in age-related macular degeneration by polarization-sensitive optical coherence tomography. *Am J Ophthalmol*. 2015;160:335–344.e1.
35. Schutze C, Wedl M, Baumann B, Pircher M, Hitzenberger CK, Schmidt-Erfurth U. Progression of retinal pigment epithelial atrophy in antiangiogenic therapy of neovascular age-related macular degeneration. *Am J Ophthalmol*. 2015;159:1100–1114.
36. Zotter S, Pircher M, Torzicky T, et al. Large-field high-speed polarization sensitive spectral domain OCT and its applications in ophthalmology. *Biomed Opt Express*. 2012;3:2720–2732.
37. Gotzinger E, Pircher M, Baumann B, et al. Speckle noise reduction in high speed polarization sensitive spectral domain optical coherence tomography. *Opt Express*. 2011;19:14568–14585.
38. Grunwald JE, Daniel E, Huang J, et al. Risk of geographic atrophy in the comparison of age-related macular degeneration treatments trials. *Ophthalmol*. 2014;121:150–161.

Investigative Ophthalmology & Visual Science